Chemical Science

ROYAL SOCIETY OF CHEMISTRY

EDGE ARTICLE

View Article Online
View Journal | View Issue

Cite this: *Chem. Sci.*, 2023, **14**, 1010

All publication charges for this article have been paid for by the Royal Society of Chemistry

Received 7th November 2022
Accepted 28th December 2022

DOI: 10.1039/d2sc06143k

rsc.li/chemical-science

Cooperatively enhanced photothermal-chemotherapy *via* simultaneously downregulating HSPs and promoting DNA alkylation in cancer cells†

Yang Zou,[a] Daipeng Huang,[a] Shan He,[c] Xuefang Song,[a] Weijian Liu,[a] Wen Sun,[ab] Jianjun Du,[ab] Jiangli Fan *[abd] and Xiaojun Peng[abd]

Photothermal therapy (PTT) has emerged as one of the important strategies for cancer treatment due to its precision and no drug resistance. However, upregulation of heat shock protein (HSP) expression during PTT severely limits its overall therapeutic effect. Accordingly, in this study, we developed a new anticancer strategy based on an L-glutathione (GSH)-activated prodrug (Cy-S-S-Cbl), which consisted of an alkylating reagent (Cbl) covalently linked to a photothermal photosensitizer (Cy7), to achieve cooperatively enhanced photothermal-chemotherapy. In the presence of overexpressed GSH in cancer cells, Cy-S-S-Cbl was converted into Cy-NH_2 to achieve photothermal effect enhancement by the photo-induced electron transfer (PET) effect and release the alkylation reagent. Meanwhile, the photothermal effect of Cy-NH_2 enhanced the DNA alkylation of chemotherapy drugs. Surprisingly, we first found that the therapeutic efficacy of PTT was improved owing to the down-regulation of heat shock protein 70 (HSP70) by chemotherapy. The two treatments had a synergistic promotion effect achieving higher cancer cell killing efficiency. Under 808 nm light irradiation, Cy-S-S-Cbl could effectively realize selective killing of cancer cells and tumor growth inhibition. Therefore, we strongly believe that this efficient cooperative design strategy will provide a new idea to improve the treatment efficiency of prodrugs.

Introduction

Photothermal therapy (PTT) is a precise, minimally invasive and low side-effect cancer treatment strategy, in which photosensitizers (PSs) convert light energy into heat through nonradiative transition to induce cancer cell necrosis.[1–6] As a heterogeneous group of molecular chaperones with various functions, heat shock proteins (HSPs) are regulated when cells are stressed in a variety of manners, especially by hyperthermia.[7–10] However, the upregulation of HSPs during PTT acts as a self-protective barrier to increase the heat resistance of cancer cells, which limits the treatment efficiency and fails to prevent tumor recurrence.[11–14] Alkylating agents, as common chemotherapy drugs, kill cancer cells by covalent binding to biological macromolecules (*e.g.*, DNA, RNA and enzymes) to inactivate them or by breaking DNA strands, which has a more thorough killing effect.[15–17] It is generally accepted that hyperthermia (>41.5 °C) caused by PTT increases the degree of DNA alkylation to enhance the cytotoxic effect of many alkylating reagents, such as chlorambucil, cyclophosphamide and ifosfamide.[18–20]

So, in most reported cases, photothermal PSs and chemotherapeutic drugs were encapsulated in nanocarriers to realize the combination of PTT and chemotherapy.[21–23] Qian *et al.* constructed docetaxel/IR780 micelles for photoacoustic/fluorescence imaging-guided photothermal-chemotherapy of breast cancer.[24] Zhu *et al.* loaded CuS nanoparticles and doxorubicin into thermosensitive nanogels for synergic PTT and chemotherapy of tumors.[25] This combination therapy system was undoubtedly more effective than either individual treatment. Nevertheless, conventional chemotherapy drugs may have severe side effects because of their low bioavailability and tumor therapeutic specificity.[26–28] Due to the uninhibited activity of photothermal PSs and chemotherapeutic drugs, they can act on various cells after being released from the nanoparticles, which may not achieve efficient selective killing of normal and cancer cells.[29–31]

The prodrug refers to the chemical modification of a drug into an inactive form with more desirable physicochemical properties and can be activated by a specific tumor microenvironment in cancer cells to its original cytotoxic form, thereby improving

[a]*State Key Laboratory of Fine Chemicals, Frontiers Science Center for Smart Materials Oriented Chemical Engineering, Dalian University of Technology, Dalian 116024, China. E-mail: fanjl@dlut.edu.cn*

[b]*Ningbo Institute of Dalian University of Technology, Ningbo 315016, China*

[c]*State Key Laboratory of Molecular Reaction Dynamics and Dynamics, Research Center for Energy and Environmental Materials, Dalian Institute of Chemical Physics Chinese Academy of Sciences, Dalian 116023, China*

[d]*Research Institute of Dalian University of Technology in Shenzhen, Shenzhen 518057, China*

† Electronic supplementary information (ESI) available. See DOI: https://doi.org/10.1039/d2sc06143k

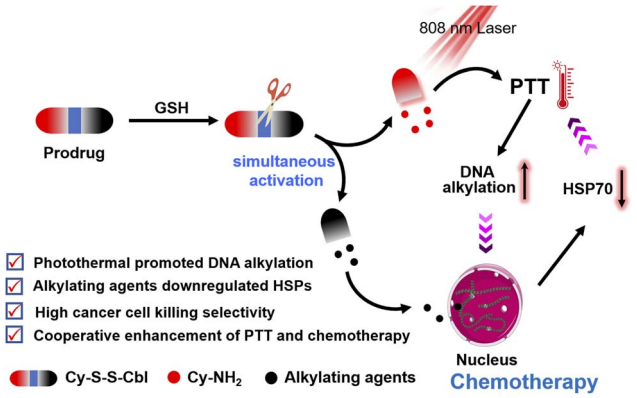

Scheme 1 Schematic illustration of Cy-S-S-Cbl based on GSH activation for cooperative enhancement of photothermal-chemotherapy.

tumor selectivity and minimizing side effects.[32–36] It has been reported that reduction-sensitive disulfide spacers can be converted to sulfhydryl groups by L-glutathione (GSH) overexpressed in cancer cells.[37–42] These prodrug strategies can selectively release chemotherapeutic drugs, while the therapeutic effect of single chemotherapy is limited. Herein, we report a new synergetic anticancer system (Cy-S-S-Cbl) based on a GSH-activated prodrug for cooperative enhancement of photothermal-chemotherapy (Scheme 1). In this prodrug, heptamethine cyanine dye (Cy7), the absorption of which was in the near infrared (NIR) region as a photothermal reagent,[43–48] was linked covalently *via* a disulfide bond to the potent DNA alkylating agent chlorambucil (Cbl),[49–52] resulting in the inhibition of both the photothermal activity of Cy7 and the chemotherapeutic activity of Cbl. As the concentration of GSH increased, the disulfide bond of Cy-S-S-Cbl was cleaved, converting the prodrug to Cy-NH_2 by intramolecular cyclization and releasing the alkylation reagent. Due to the photo-induced electron transfer (PET) effect, the fluorescence of Cy-NH_2 was significantly quenched, resulting in the release of absorbed energy mainly by heat and higher photothermal conversion efficiency than Cy-S-S-Cbl. Meanwhile, the photothermal effect of Cy-NH_2 enhanced the DNA alkylation of Cbl, thereby promoting the chemotherapy effect. Interestingly, we first found that in the presence of Cbl, the effect of PTT was much improved as well due to the reduction of the HSP70 expression, which meant that the two treatments had a synergistic promotion effect, achieving excellent selectivity and killing ability for cancer cells. Under 808 nm light irradiation, Cy-S-S-Cbl could effectively realize tumor inhibition and had no detectable side effects on normal tissue. Therefore, we believe that this efficient cooperative design approach will provide a new prodrug strategy for cancer treatment.

Results and discussion

Design, synthesis and photochemical properties

Based on our previous study, replacing the chlorine atom in the middle position of heptamethine cyanine dyes with a 4-aminobenzyl thio group induced the photo-induced electron transfer (PET) effect, resulting in fluorescence quenching accompanied by an increased proportion of non-radiative relaxation.[45,53] Meanwhile, sulfonate groups were introduced into the cyanine dye skeleton to improve the water solubility. Subsequently, the amino group was linked to the chemotherapy drug (Cbl) *via* acylation with the classical disulfide bond drug-releasing group, which was designed as an activatable prodrug (Cy-S-S-Cbl). With the increasing concentration of GSH, Cy-S-S-Cbl can be readily converted into a molecule (Cy-NH_2) and released chemotherapy drugs. As shown in Scheme S1, Cy-S-S-Cbl and Cy-NH_2 were synthesized, and Cy-NH_2 was used as the control molecule to better understand our concept. The chemical structures of Cy-S-S-Cbl, Cy-NH_2 and all synthetic intermediates were confirmed by ^{1}H NMR, ^{13}C NMR, and ESI-HRMS analytical data (Fig. S16–S24†).

The UV-vis absorbance spectrum showed that both Cy-S-S-Cbl and Cy-NH_2 presented strong absorption ranging from 700 to 850 nm in the near infrared (NIR) region and the molar extinction coefficients were nearly 2×10^5 M^{-1} cm^{-1} (Fig. 1a). Upon 730 nm excitation, the fluorescence of Cy-NH_2 at 820 nm was greatly quenched ($\Phi_f = 0.5\%$) and was much weaker than that of Cy-S-S-Cbl ($\Phi_f = 4.6\%$) (Fig. 1b and Table 1). To explain the large difference, a femtosecond transient absorption (TA) assay was performed to further confirm the existence of "PET-induced emission quenching" and "PET blocking" processes in Cy-NH_2 and Cy-S-S-Cbl, respectively. The TA kinetics of Cy-NH_2 was fitted with three

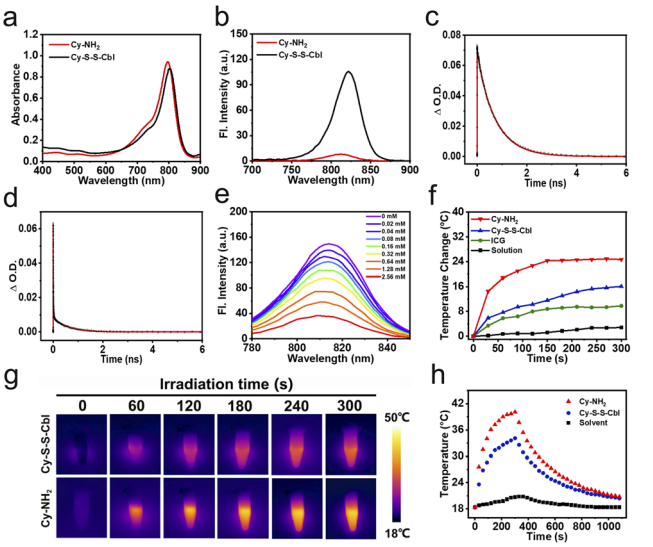

Fig. 1 (a) Absorption spectra and (b) fluorescence spectra of Cy-S-S-Cbl and Cy-NH_2. Decay kinetics according to a femtosecond pump-probe of (c) Cy-S-S-Cbl and (d) Cy-NH_2. Excited with an 800 nm pulsed laser. (e) The emission changes of Cy-S-S-Cbl (10 μM) with different concentrations of GSH in PBS buffer solutions (0.01 M PBS, PBS/DMSO = 8 : 2 v/v) over time. (f) Photothermal temperature change curves of Cy-NH_2, Cy-S-S-Cbl, ICG and solution at the same concentration (40 μM) under 808 nm light irradiation (0.5 W cm^{-2}), respectively. (g) Photothermal imaging of Cy-S-S-Cbl and Cy-NH_2 in the PBS buffer solutions (0.01 M PBS, PBS/DMSO = 8 : 2 v/v) at 40 μM concentration under 808 nm light (0.5 W cm^{-2}) irradiation. (h) Photothermal effects observed upon Cy-S-S-Cbl or Cy-NH_2 with 808 nm light (0.5 W cm^{-2}) irradiation for 300 s, and then the light was switched off.

Table 1 Photophysical properties of Cy-S-S-Cbl and Cy-NH_2 [a]

Molecular	λ_{abs} (nm)	λ_{em} (nm)	ε ($\times 10^4$ M^{-1} cm^{-1})	Φ_f (%)	η (%)
Cy-S-S-Cbl	804	822	21.9	4.6	26.35
Cy-NH_2	797	812	23.6	0.5	43.15

[a] λ_{abs}: absorption maximum wavelength (nm). λ_{em}: emission maximum wavelength (nm). ε: molar extinction coefficient (10^4 M^{-1} cm^{-1}). Φ_f: fluorescence quantum yield. η: photothermal conversion efficiency.

Table 2 Fitting parameters from TA kinetics

compd	A_1 [a](%)	τ(ps)[b]	A_2 [a](%)	τ(ps)[b]	A_3 [a](%)	τ(ps)[b]
Cy-S-S-Cbl	93.9	743	5.3	123	0.8	26.8
Cy-NH_2	12.4	573	24	14	63.6	2.04

[a] A: the fraction of excited population of the associated component. [b] τ (ps): lifetime.

time-components: $\tau_1 = 573$ ps (12.4%), $\tau_2 = 14$ ps (24%), and an ultrashort lifetime $\tau_3 = 2.04$ ps (63.6%) (Fig. 1c and d, and Table 2). Meanwhile, there were three time-components for Cy-S-S-Cbl (93.9% for $\tau_1 = 743$ ps, 5.3% for $\tau_2 = 123$ ps and 0.8% for $\tau_2 = 26.8$ ps). The timescales τ_1 of Cy-NH_2 and τ_1 and τ_2 of Cy-S-S-Cbl can be attributed to the lifetime of the S1 state, and τ_2 of Cy-NH_2 and τ_3 of Cy-S-S-Cbl can be attributed to the lifetime of vibrational cooling processes, respectively. In contrast to Cy-S-S-Cbl, there was an ultrafast process (2.04 ps) after most of the electrons in Cy-NH_2 were activated from the ground state to the excited state, during which (2.04 ps) they were plundered to the PET state, resulting in non-radiative relaxation. These results confirmed that Cy-NH_2 had a stronger PET effect than Cy-S-S-Cbl, resulting in fluorescence quenching.

Activable properties

Subsequently, we explored the reaction mechanism of Cy-S-S-Cbl and GSH. The possible GSH-activated product of Cy-S-S-Cbl may be Cy-NH_2 and drugs (Scheme 2). To verify this, the response of Cy-S-S-Cbl toward GSH was tested in PBS solution (0.01 M, PBS/DMSO = 8 : 2, v/v, and pH = 7.4). As the GSH concentration increased (0 mM to 2.56 mM), the fluorescence intensity of Cy-S-S-Cbl gradually decreased (Fig. 1e). Upon the addition of GSH (250 equiv., 2.5 mM), the fluorescence of Cy-S-S-Cbl significantly decreased with the increase of reaction time and showed a slight blue-shift (Fig. S1†). We speculated that the large fluorescence change was attributed to the transformation of Cy-S-S-Cbl to Cy-NH_2. Then, the reaction products were determined by ESI-MS analysis. The mass peaks of Cy-S-S-Cbl ($m/z = 1279.83$ for $[M - Na]^-$) and Cy-NH_2 ($m/z = 814.16$ for $[M - Na]^-$) were detected simultaneously (Fig. S2†). Furthermore, the HPLC chromatogram was used to further validate the products. As shown in Fig. S3,† the peak of Cy-S-S-Cbl (retention time 17 min) decreased, while the peak of Cy-NH_2 (retention time 26.8 min) and drug (retention time 22.1 min) appeared after 1 h reaction with GSH. These results confirmed that GSH triggered

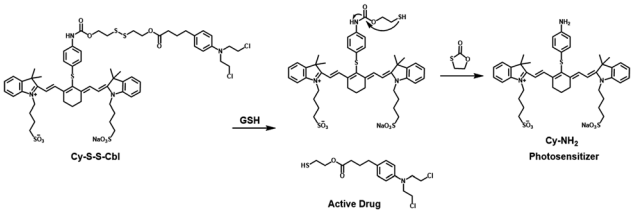

Scheme 2 Proposed Cy-NH_2 and drug release mechanism of the activable Cy-S-S-Cbl by GSH.

the disulfide cleavage of Cy-S-S-Cbl to release Cy-NH_2 and drugs. Meanwhile, the drug release efficiency of Cy-S-S-Cbl with GSH was significantly higher than that without GSH (Fig. S4†). Moreover, Cy-S-S-Cbl displayed high selectivity for biothiols, such as GSH and Cys, without any interference from other biological species, including metal ions (K^+, Ca^{2+}, Na^+, and Mg^{2+}) and bioactive small molecules (Ala, Arg, Glu, Ser, Thr, Trp, and Tyr) (Fig. S5†).

Photothermal performance

Next, we further examined the photothermal properties of Cy-NH_2 by monitoring the temperature changes over time in PBS buffer solution (0.01 M PBS, PBS/DMSO = 7 : 3 v/v, and pH = 7.4) under different power densities and at different concentrations. The Cy-NH_2 solution (40 μM) was irradiated with 808 nm light at different power densities from 0 W cm^{-2} to 0.6 W cm^{-2} for 5 min (Fig. S6a†). The solution temperature increased gradually with the increase of light intensity, and the final temperature increased slowly when the power densities reached 0.6 W cm^{-2}. Therefore, we selected an appropriate power density of 0.5 W cm^{-2} for the subsequent experiments. Furthermore, the temperature increase of the Cy-NH_2 solution was positively correlated with the Cy-NH_2 concentration from 0 μM to 40 μM after irradiation with 808 nm light (0.5 W cm^{-2}) (Fig. S6b†). Then, the photothermal properties of different components, Cy-NH_2, Cy-S-S-Cbl and indocyanine green (ICG) solutions at the same concentration were evaluated under light irradiation, respectively (Fig. 1f and g). As expected, due to the PET effect, the temperature increase of Cy-NH_2 was higher than that of other groups, and the photothermal conversion efficiency (η) of Cy-NH_2 was approximately 43.2%, which was much higher than that of Cy-S-S-Cbl (26.4%) (Fig. 1h). In addition, photostability is also an important factor affecting the photothermal properties of PSs. The production of reactive oxygen species (ROS) during light irradiation can decrease the stability of Cy7 dramatically and may adversely affect normal cells.[54,55] Thus, singlet oxygen sensor green (SOSG) and 9,10-anthracenediyl-bis-(methylene) dimalonic acid (ABDA) were used to test the $^1O_2$ generation ability of Cy-NH_2 and Cy-S-S-Cbl, respectively. The fluorescence of SOSG and absorption of ABDA did not change substantially in the presence of Cy-NH_2 or Cy-S-S-Cbl under 808 nm light irradiation, indicating that no ROS were generated (Fig. S7 and S8†). What's more, the reductions in the absorbances of Cy-NH_2 and Cy-S-S-Cbl were significantly lower than that of ICG after irradiation, which directly demonstrated that they had better

stability (Fig. S9†). Both the above-mentioned results confirmed that Cy-NH_2 had excellent properties as a photothermal agent.

Cytotoxicity evaluation of Cy-S-S-Cbl

The biocompatibility and activable properties of Cy-S-S-Cbl at the cellular level were investigated in both cancer (HeLa, HepG2, MCF-7 and 4T1) and normal (3T3) cell lines. First, the GSH concentration of different kinds of cells was investigated by using the Reduced Glutathione (GSH) Content Assay Kit. As shown in Fig. S10,† the GSH concentration of cancer cells was approximately 10-times higher than that of normal (3T3) cells. Then, the cell uptake of Cy-S-S-Cbl was examined by fluorescence confocal microscopy. As expected, the red fluorescence of Cy-S-S-Cbl in HeLa cells was weaker than that in 3T3 cells after 4 h of incubation, revealing that the fluorescence of Cy-S-S-Cbl was partially quenched (Fig. S11†). When the cells were first incubated with *N*-ethylmaleimide (NEM), a thiol scavenging agent, and then Cy-S-S-Cbl was added, the fluorescence of HeLa and 3T3 cells was similar and was stronger than that of the cells incubated without NEM. This finding demonstrated that Cy-S-S-Cbl was taken up by cells efficiently and interacted with overexpressed GSH in cancer cells. Furthermore, glutathione disulfide (GSSG) is the product of GSH after oxidation which is often used together to measure changes in the GSH content. The intracellular relative GSH/GSSG ratios in HeLa and 4T1 cells were substantially decreased after treatment with Cy-S-S-Cbl, whereas no obvious changes were observed after incubating with PBS or Cy-NH_2 (Fig. 2a). These results demonstrated that Cy-NH_2 could be transformed from Cy-S-S-Cbl only in cancer cells by consuming high levels of GSH.

A prodrug that can be activated efficiently in cancer cells could reduce biotoxicity and improve therapeutic efficacy. To evaluate the potential application of Cy-S-S-Cbl in selective killing of cancer cells, the *in vitro* inhibition of cell proliferation by Cy-S-S-Cbl was tested using the methyl thiazolyltetrazolium (MTT) assay. As shown in Fig. 2b, the cell viability of cells treated with Cy-S-S-Cbl was lower than those of cells treated with Cy-NH_2 and Cy-S-S-Cbl + NEM, which demonstrated that the cytotoxicity was attributed to the release of drugs due to the breakage of disulfide bonds by GSH, indicating that Cy-S-S-Cbl had excellent biocompatibility. After irradiation with 808 nm light (0.5 W cm^{-2}) for 5 min, the cell viability of cells incubated with Cy-S-S-Cbl decreased to 14%, which was significantly lower than those of cells incubated with Cy-NH_2 and Cy-S-S-Cbl + NEM, suggesting a considerable improvement in the killing effect in cancer cells (Fig. 2c). The same method was applied in other cancer and normal cells. The results showed that Cy-S-S-Cbl had a much higher biotoxicity for cancer cells (HepG2, MCF-7 and 4T1) than for normal cells (3T3), whereas Cy-NH_2 had the same toxicity to all kinds of cells, indicating the excellent killing selectivity of Cy-S-S-Cbl and biosecurity of Cy-NH_2 (Fig. S12†). Compared with the cell viability after different treatments, it's worth noting that the cell survival of the Cy-S-S-Cbl + Light group was 14.62 ± 1.39%, which was lower than the sum of the cell survivals for the Cbl (87.1 ± 3.25% cell survival) and Cy-NH_2 + Light (38.53 ± 4.08% cell survival) groups, demonstrating that the cooperative chemotherapy/PTT mechanism was involved in killing the cancer cells and achieved a better killing effect (Fig. 2d). Subsequently, HeLa cells were stained with propidium iodide (PI, red fluorescence) and calcein-AM (green fluorescence) to observe dead and live cells more intuitively. Clearly, nearly all cells treated with Cy-S-S-Cbl under 808 nm light irradiation showed strong red fluorescence, revealing more dead cells than for the cells treated with Cy-S-S-Cbl + NEM under 808 nm light irradiation (Fig. 2e). In comparison, very weak red fluorescent signals and strong green fluorescence were observed in the other groups, which indicated that most cells were alive. The excellent killing effect of Cy-S-S-Cbl was also observed in the other cancer cells under the same conditions (Fig. S13†). Next, flow cytometry with Annexin V-FITC and propidium iodide (PI) was used to evaluate the apoptosis and necrosis rates. AV staining of the membrane indicated the early stage of cell apoptosis, and PI staining of the nucleus indicated late apoptotic or dead cells. The necrosis ratios for HeLa cells after treatment with Cy-S-S-Cbl and Cy-NH_2 under 808 nm (0.5 W cm^{-2}) light irradiation were 29.3% and 19.5%,

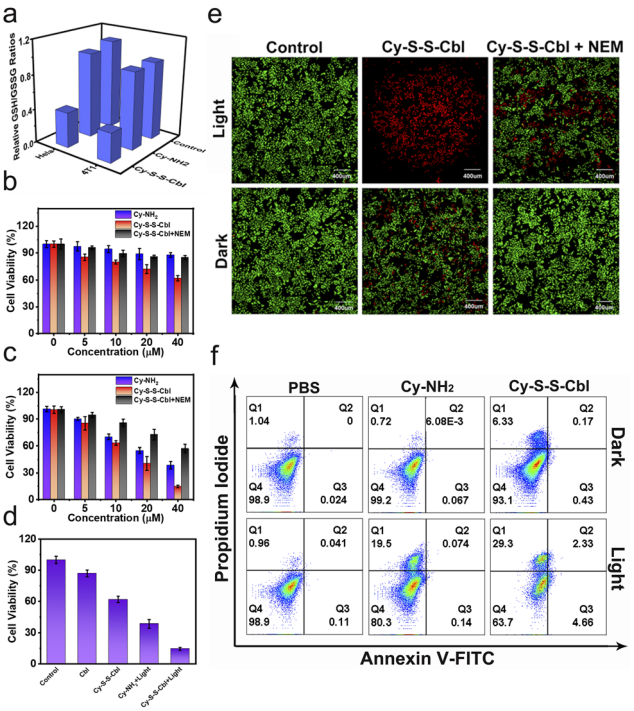

Fig. 2 (a) Relative GSH/GSSG ratios in HeLa and 4T1 cells under different conditions. *Ex vivo* survival rate of HeLa cells after incubation with Cy-NH_2, Cy-S-S-Cbl or Cy-S-S-Cbl + NEM at different concentrations in the dark (b) or with 808 nm light irradiation (0.5 W cm^{-2}) for 5 min (c). (d) Cytotoxicity evaluation of HeLa cells with Cbl, Cy-NH_2 or Cy-S-S-Cbl treatment under different conditions. (e) Calcein AM and propidium iodide (PI) co-staining fluorescence imaging in HeLa cells. (f) Flow cytometry analysis by Annexin V-FITC and PI staining of HeLa cells following different treatments. Cells were incubated under different conditions and divided into six groups, including (1) control, (2) 808 nm light irradiation, (3) Cy-NH_2, (4) Cy-NH_2 with 808 nm light irradiation, (5) Cy-S-S-Cbl and (6) Cy-S-S-Cbl with 808 nm light irradiation. Scale bar: 400 μm.

respectively (Fig. 2f). Simultaneously, no obvious killing effect was observed for HeLa cells treated with light or PSs alone (cell viability >93%). Thus, we demonstrated that the killing effect of Cy-S-S-Cbl in tumor cells was considerably improved owing to the cooperative effect of PTT and chemotherapy.

Cooperative mechanism of PTT and chemotherapy

Such an improvement in the killing effect of cancer cells prompted us to investigate the cooperative mechanism of PTT and chemotherapy. First, the alkylation mechanism of chemotherapeutic drugs was explored. Since Cbl is a DNA alkylating agent, the ability of Cy-S-S-Cbl to interact with DNA after incubation with GSH was evaluated *in vitro* with plasmid DNA (pBR322) by agarose gel electrophoresis (Fig. 3a).[56,57] The unreacted supercoiled plasmid DNA was present in the lower band, which exhibited a dose-dependent decrease in accordance with the formation of alkylated DNA in the higher band. After incubation with 10 mM GSH at 37 °C for 12 h, the DNA alkylation rate of Cy-S-S-Cbl at 100 μM concentration was nearly 100%, which was similar to that of the Cbl group, and the alkylation efficiency increased gradually with the increase of Cy-S-S-Cbl concentrations. However, after incubation with GSH and Cy-NH_2, plasmid DNA basically existed in the form of a double-stranded superhelix, which was similar to the reference. This result suggested that alkylation reagents could be released by Cy-S-S-Cbl to trigger DNA damage. To further evaluate the damage to cellular DNA caused by Cy-S-S-Cbl, a comet assay was visually performed on HeLa cells (Fig. 3b). After incubation with Cy-S-S-Cbl for 4 h at 37 °C, substantial comet trailing was observed by fluorescence microscopy (propidium iodide (PI) staining), indicating DNA strand breaks and short DNA fragment migrations. Meanwhile, the extent of cellular DNA damage increased with the increased concentrations (10–40 μM) of Cy-S-S-Cbl, revealing that the released drug reached the target DNA inside the cell and damaged the DNA. Moreover, as DNA interstrand cross-links can block replication and transcription completely and double stand breaks (DSBs) may also be generated during its repair, γ-H2AX immuno-fluorescence microscopy was a well-accepted and sensitive method to detect DSBs.[58] As shown in Fig. 3c and Fig. S14,† the incubation of Cy-S-S-Cbl (40 μM) triggered prominent red γ-H2AX fluorescence in the HeLa cell nucleus, revealing the generation of DNA damage. However, no noticeable DNA damage was observed in the Cy-NH_2 and control groups. These results confirmed that drugs released by Cy-S-S-Cbl could damage DNA by the alkylation effect. Recently, several studies have reported that hyperthermia can increase the degree of DNA alkylation.[18–20] After incubation with 10 mM GSH for 12 h at 37 °C, the DNA alkylation ratio for Cy-S-S-Cbl under 808 nm light irradiation was higher than for Cy-S-S-Cbl in the dark (Fig. 3d). In addition, the DNA alkylation ratio of Cy-NH_2 with and without irradiation was very low and the difference was not significant due to the absence of the alkylation effect. Therefore, the result showed that PTT promoted the chemotherapeutic effect of alkylation reagents. Since the expression of HSPs is an important factor affecting the photothermal effect, a western blotting assay was performed to explore the effect of chemotherapeutic drugs on HSP70, which is the most important and the most sensitive to temperature, in cells after different treatments. Interestingly, we found that cells treated with Cy-S-S-Cbl downregulated HSP70 after 808 nm light irradiation compared with those treated with Cy-NH_2 and irradiation, which was able to block the PTT-resistance pathway achieving chemotherapy-enhanced PTT (Fig. 3e). Similar results were also obtained in immunofluorescence (Fig. 3c) and MTT assays (Fig. 2d). These results confirmed that our strategy can effectively achieve the cooperative enhancement of PTT and chemotherapy.

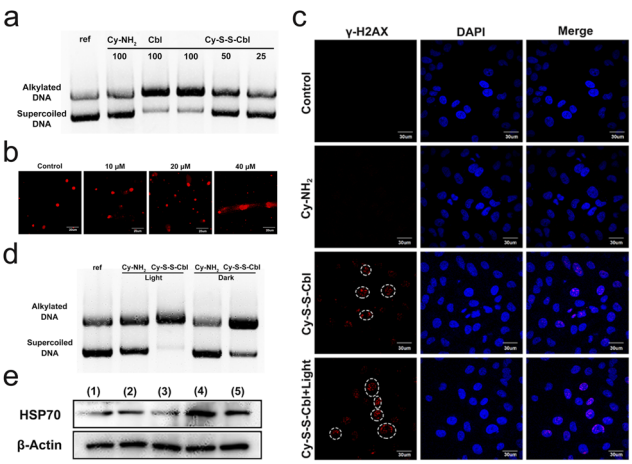

Fig. 3 (a) Agarose gel of plasmid DNA (pBR322) incubated at 37 °C for 4 h with different concentrations of Cy-S-S-Cbl (25, 50, and 100 μM) or Cy-NH_2 (100 μM) in the presence of 10 mM GSH and Cbl (100 μM), respectively. (b) Alkaline comet assay for HeLa cells treated with Cy-S-S-Cbl (10, 20 and 40 μM) for 4 h. Nuclear DNA was stained with PI (propidium iodide, a red fluorescent dye). Scale bar: 20 μm. (c) γ-H2AX immunofluorescence in HeLa cells with different treatments, including Cy-NH_2, Cy-S-S-Cbl, and Cy-S-S-Cbl + light. The white dotted circles indicate γ-H2AX foci (red) and the hoechst 33 258 dye (blue) localizes the nuclear DNA. Scale bar: 30 μm. (d) Agarose gel of plasmid DNA (pBR322) incubated at 37 °C for 4 h with Cy-S-S-Cbl or Cy-NH_2 (50 μM) in the presence of 10 mM GSH with/without 808 nm light irradiation. (e) Western blot analysis of HSP70 expression in HeLa cells after different treatments. Different groups: (1) PBS, (2) PBS + 808 nm light, (3) Cy-S-S-Cbl, (4) Cy-NH_2 + 808 nm light and (5) Cy-S-S-Cbl + 808 nm light.

In vivo application

The excellent tumoricidal efficiency of Cy-S-S-Cbl at the cell level inspired us to further evaluate its therapeutic effect *in vivo*. HeLa tumor-bearing SCID/BALB/c-nude mice were constructed as the model. Compared with the tumor directly injected with Cy-S-S-Cbl, the NEM preinjection group exhibited stronger NIR fluorescence during all periods, and both groups reached the maximum fluorescence at approximately 4 h post-injection (Fig. 4a and b). Therefore, the light irradiation was implemented at 4 h after the intratumoral injection to maximize the therapeutic effect. The photothermal efficacy of Cy-S-S-Cbl in HeLa tumor-bearing mice was evaluated by the changes in tumor temperature against time. In order to avoid the influence on surrounding normal tissues caused by long time and

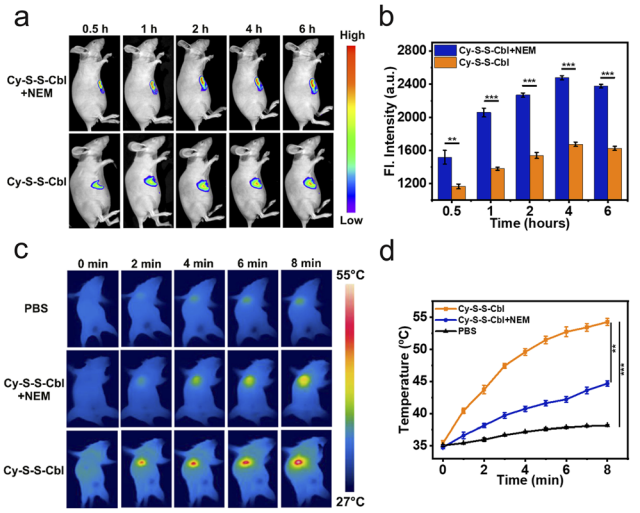

Fig. 4 (a) *In vivo* fluorescence imaging of HeLa tumor-bearing SCID/BALB/c-nude mice after intratumoral injection of Cy-S-S-Cbl or Cy-S-S-Cbl + NEM at 0.5, 1, 2, 4, and 6 h. (b) Fluorescence intensities of Cy-S-S-Cbl or Cy-S-S-Cbl + NEM for tumor sites at different time points, which were the quantitative data of (a). (c) IR thermal images of HeLa tumor-bearing SCID/BALB/c-nude mice following 808 nm light irradiation (0.5 W cm^{-2}) at different time points. The laser exposure was performed at 4 h after the injection of 100 μL (300 μM L^{-1}) PBS, Cy-S-S-Cbl + NEM or Cy-S-S-Cbl. (d) Temperature changes at the tumor sites as a function of the 808 nm light (0.5 W cm^{-2}) irradiation time, which are the quantitative data of (c). Error bars, mean ± SD ($n = 4$), $^{**}P < 0.01$, and $^{***}P < 0.001$ determined by Student's *t*-test.

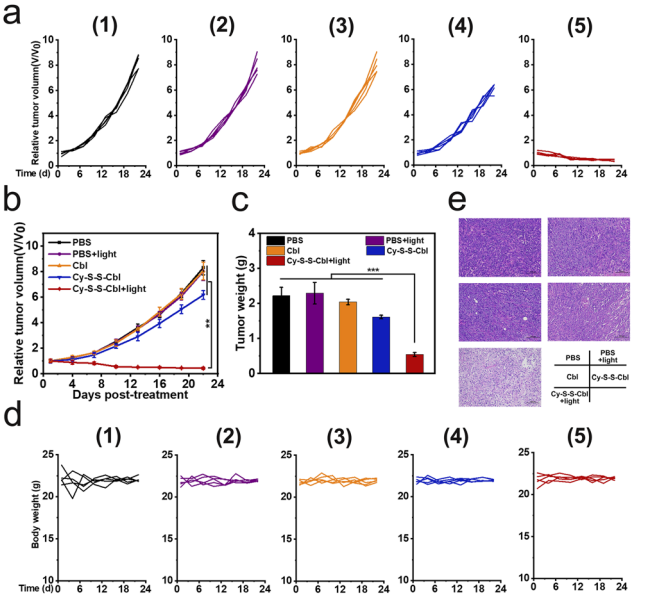

Fig. 5 Anti-tumor activity of Cy-S-S-Cbl in HeLa tumor-bearing SCID/BALB/c-nude mice. (a) Individual tumor growth curves in different treatment groups. (b) Average tumor growth curves in different treatment groups. (c) Tumor weight for mice in different treatment groups. (d) Individual weight changes of mice in a subcutaneous tumor animal model over 21 days of treatment. (e) H&E stained tumor sections from the indicated treatment groups. Scale bars = 100 μm. Different groups: (1) PBS; (2) PBS + 808 nm light; (3) Cbl; (4) Cy-S-S-Cbl; (5) Cy-S-S-Cbl + 808 nm light. Data are shown as mean ± SD ($n = 5$), $^{**}P < 0.01$, and $^{***}P < 0.001$ determined by Student's *t*-test.

frequent exposure to 808 nm light, we adopted one-time irradiation for 8 minutes. The temperature of tumors in the Cy-S-S-Cbl + 808 nm light ($\Delta T \approx 19$ °C) group rapidly increased and was much higher than that in the Cy-S-S-Cbl pre-injected with NEM + 808 nm light ($\Delta T \approx 9$ °C) group (Fig. 4c and d), while the temperature in the blank PBS buffer group barely changed. Actually, temperature below 42 °C does not kill tumor cells efficiently by the photothermal effect.[59] Clearly, the considerably elevated temperature of the Cy-S-S-Cbl treated tumors under irradiation was indeed associated with endogenous GSH in the tumors. Therefore, Cy-S-S-Cbl demonstrated effective *in vivo* photothermal conversion for PTT.

Based on these results, we investigated the therapeutic efficacy of Cy-S-S-Cbl *in vivo* further in HeLa tumor-bearing SCID/BALB/c-nude mice, which were randomly divided into the following five groups ($n = 5$): PBS; PBS + light; Cbl; Cy-S-S-Cbl; Cy-S-S-Cbl + light. The mice were intratumorally injected with the different reagents, and then after 4 h they were irradiated with 808 nm light (0.5 W cm^{-2}) for 8 min. The *in vivo* antitumor effects of the different treatments were evaluated according to the change in tumor volume measured every other day over 21 days (calculated from the next day after treatment). A negligible inhibitory effect on the tumor was observed in the PBS, PBS + light, and Cbl groups (tumor growth of *ca.* 8-fold), whereas a slight or moderate tumor inhibition effect was observed in the Cy-S-S-Cbl group (tumor growth of *ca.* 6-fold) because of sole Cbl-mediated chemotherapy (Fig. 5a–c). Notably, the Cy-S-S-Cbl + light group showed a reduction in tumor volume and successful inhibition in tumor growth after only one treatment, which indicated an excellent synergistic treatment effect. The safety of the prodrug in organisms is an important index to evaluate whether it can be applied in biomedical applications. The weights of all the mice in the intratumoral injection groups remained constant, indicating that the treatments did not affect the normal physiological activities of the mice (Fig. 5d). In addition, the major organs of each group, including the heart, liver, spleen, lung, kidney and tumor tissues, were prepared for hematoxylin and eosin (H&E) staining. The tumor slices from the Cy-S-S-Cbl + light group showed obvious necrosis (Fig. 5e) and no obvious damage or toxicity to other tissues, demonstrating the biosafety of the prodrug for normal tissues (Fig. S15†). Overall, these results comprehensively demonstrated the biocompatibility and biosafety of Cy-S-S-Cbl *in vivo*, indicating its potential clinical application significance.

Conclusions

In summary, we developed a new strategy for designing an effective anticancer system based on a GSH-activated prodrug for cooperative enhancement of photothermal-chemotherapy. As the GSH concentration increased, Cy-S-S-Cbl was converted into Cy-NH_2 to enhance the photothermal effect by PET quenching fluorescence and released the alkylation reagent at the same time. Cy-S-S-Cbl achieved a considerable improvement

in the cancer cell killing effect compared with free Cy-NH_2 under irradiation. What's more, the photothermal effect of Cy-NH_2 enhanced the DNA alkylation of chemotherapy drugs. Importantly, we first found and demonstrated that chemotherapy improved the efficacy of PTT by down-regulating the expression of HSP70, which meant that the two treatments showed synergistic promotion to achieve higher cancer cell killing efficiency and selectivity. Under 808 nm light irradiation, Cy-S-S-Cbl could effectively realize tumor inhibition and had no detectable side effects in normal tissue. Therefore, we strongly believe that this efficient cooperative design strategy will provide a new idea for improving the treatment efficiency of prodrugs with potential clinical application prospects.

Data availability

The ESI† include the synthesis, NMR and high-resolution mass spectrometry of photosensitizers, the experiment of cell uptake, live/dead cell staining, mouse phototherapy, biosafety tests, *etc.*

Author contributions

Y. Zou designed and performed all the experiments and wrote the manuscript. D. P. Huang, S. He and X. F. Song participated in some experiments. W. J. Liu carried out and participated in TOC drawing. J. L. Fan directed the whole process in this work, guided the writing and revised the manuscript. J. L. Fan, W. Sun, J. J. Du, and X. J. Peng offered constructive suggestions on the improvement of this work and provided financial support.

Conflicts of interest

The authors declare no competing financial interests.

Acknowledgements

This work was supported by the National Natural Science Foundation of China (21925802, 21421005, 22090010 and 22022803), the Fundamental Research Fundamental Funds for the Central Universities (DUT22LAB601), and the NSFC-Liaoning United Fund (U1908202). This study was conducted in accordance with the Guide for the Care and Use of Laboratory Animals published by the US National Institutes of Health (8th edition, 2011). The animal protocol was approved by the local research ethics review board of the Animal Ethics Committee of Dalian University of Technology.

Notes and references

1 Y. Liu, P. Bhattarai, Z. Dai and X. Chen, *Chem. Soc. Rev.*, 2019, **48**, 2053–2108.
2 X. Wei, C. Zhang, S. He, J. Huang, J. Huang, S. S. Liew, Z. Zeng and K. Pu, *Angew. Chem., Int. Ed.*, 2022, **61**, e202202966.
3 P. Cheng and K. Pu, *Nat. Rev. Mater.*, 2021, **6**, 1095–1113.
4 D. Xi, M. Xiao, J. Cao, L. Zhao, N. Xu, S. Long, J. Fan, K. Shao, W. Sun, X. Yan and X. Peng, *Adv. Mater.*, 2020, **32**, e1907855.
5 H. B. Cheng, H. Dai, X. Tan, H. Li, H. Liang, C. Hu, M. Huang, J. Y. Lee, J. Zhao, L. Zhou, Y. Wang, L. Zhang and J. Yoon, *Adv. Mater.*, 2022, **34**, e2109111.
6 H. Gu, W. Liu, W. Sun, J. Du, J. Fan and X. Peng, *Chem. Sci.*, 2022, **13**, 9719–9726.
7 R. I. Morimoto and M. G. Santoro, *Nat. Biotechnol.*, 1998, **16**, 833–838.
8 J. Wu, T. Liu, Z. Rios, Q. Mei, X. Lin and S. Cao, *Trends Pharmacol. Sci.*, 2017, **38**, 226–256.
9 M. Jaattela, *Ann. Med.*, 1999, **31**, 261–271.
10 S. Jindal, *Trends Biotechnol.*, 1996, **14**, 17–20.
11 Y. Yang, W. Zhu, Z. Dong, Y. Chao, L. Xu, M. Chen and Z. Liu, *Adv. Mater.*, 2017, **29**, 1703588.
12 J. Peng, Y. Xiao, W. Li, Q. Yang, L. Tan, Y. Jia, Y. Qu and Z. Qian, *Adv. Sci.*, 2018, **5**, 1700891.
13 C. Wang, L. Xu, C. Liang, J. Xiang, R. Peng and Z. Liu, *Adv. Mater.*, 2014, **26**, 8154–8162.
14 Q. Dong, X. Wang, X. Hu, L. Xiao, L. Zhang, L. Song, M. Xu, Y. Zou, L. Chen, Z. Chen and W. Tan, *Angew. Chem., Int. Ed.*, 2018, **57**, 177–181.
15 D. Fu, J. A. Calvo and L. D. Samson, *Nat. Rev. Cancer*, 2012, **12**, 104–120.
16 K. Onizuka, M. E. Hazemi, N. Sato, G. I. Tsuji, S. Ishikawa, M. Ozawa, K. Tanno, K. Yamada and F. Nagatsugi, *Nucleic Acids Res.*, 2019, **47**, 6578–6589.
17 A. M. Chiorcea-Paquim and A. M. Oliveira-Brett, *J. Pharm. Biomed. Anal.*, 2023, **222**, 115036.
18 N. van den Tempel, M. R. Horsman and R. Kanaar, *Int. J. Hyperthermia*, 2016, **32**, 446–454.
19 R. D. Issels, *Eur. J. Cancer*, 2008, **44**, 2546–2554.
20 A. L. Oei, L. E. Vriend, J. Crezee, N. A. Franken and P. M. Krawczyk, *Radiat. Oncol.*, 2015, **10**, 165.
21 W. Fan, B. Yung, P. Huang and X. Chen, *Chem. Rev.*, 2017, **117**, 13566–13638.
22 H. Sun, Q. Zhang, J. Li, S. Peng, X. Wang and R. Cai, *Nano Today*, 2021, **37**, 101073.
23 T. T. Zhang, C. H. Xu, W. Zhao, Y. Gu, X. L. Li, J. J. Xu and H. Y. Chen, *Chem. Sci.*, 2018, **9**, 6749–6757.
24 W. Li, J. Peng, Q. Yang, L. Chen, L. Zhang, X. Chen and Z. Qian, *Biomater. Sci.*, 2018, **6**, 1201–1216.
25 Z. Meng, F. Wei, R. Wang, M. Xia, Z. Chen, H. Wang and M. Zhu, *Adv. Mater.*, 2016, **28**, 245–253.
26 K. Cho, X. Wang, S. Nie, Z. G. Chen and D. M. Shin, *Clin. Cancer Res.*, 2008, **14**, 1310–1316.
27 S. Y. Qin, A. Q. Zhang, S. X. Cheng, L. Rong and X. Z. Zhang, *Biomaterials*, 2017, **112**, 234–247.
28 K. Nurgali, R. T. Jagoe and R. Abalo, *Front. Pharmacol.*, 2018, **9**, 245.
29 P. Huang, D. Wang, Y. Su, W. Huang, Y. Zhou, D. Cui, X. Zhu and D. Yan, *J. Am. Chem. Soc.*, 2014, **136**, 11748–11756.
30 X. Meng, J. Zhang, Z. Sun, L. Zhou, G. Deng, S. Li, W. Li, P. Gong and L. Cai, *Theranostics*, 2018, **8**, 6025–6034.
31 C. Yan, Z. Guo, Y. Shen, Y. Chen, H. Tian and W. H. Zhu, *Chem. Sci.*, 2018, **9**, 4959–4969.
32 A. G. Cheetham, R. W. Chakroun, W. Ma and H. Cui, *Chem. Soc. Rev.*, 2017, **46**, 6638–6663.

33 M. H. Lee, A. Sharma, M. J. Chang, J. Lee, S. Son, J. L. Sessler, C. Kang and J. S. Kim, *Chem. Soc. Rev.*, 2018, **47**, 28–52.
34 X. Dong, R. K. Brahma, C. Fang and S. Q. Yao, *Chem. Sci.*, 2022, **13**, 4239–4269.
35 E. J. Kim, S. Bhuniya, H. Lee, H. M. Kim, C. Cheong, S. Maiti, K. S. Hong and J. S. Kim, *J. Am. Chem. Soc.*, 2014, **136**, 13888–13894.
36 Y. Yuan, R. T. Kwok, B. Z. Tang and B. Liu, *J. Am. Chem. Soc.*, 2014, **136**, 2546–2554.
37 M. H. Lee, Z. Yang, C. W. Lim, Y. H. Lee, S. Dongbang, C. Kang and J. S. Kim, *Chem. Rev.*, 2013, **113**, 5071–5109.
38 C. Hwang, A. J. Sinskey and H. F. Lodish, *Science*, 1992, **257**, 1496–1502.
39 M. H. Lee, J. L. Sessler and J. S. Kim, *Acc. Chem. Res.*, 2015, **48**, 2935–2946.
40 X. Wu, X. Sun, Z. Guo, J. Tang, Y. Shen, T. D. James, H. Tian and W. Zhu, *J. Am. Chem. Soc.*, 2014, **136**, 3579–3588.
41 D. Huang, H. Huang, M. Li, J. Fan, W. Sun, J. Du, S. Long and X. Peng, *Adv. Funct. Mater.*, 2022, 202208105.
42 X. Li, Y. Hou, J. Zhao, J. Li, S. Wang and J. Fang, *Chem. Sci.*, 2020, **11**, 3215–3222.
43 W. Sun, S. Guo, C. Hu, J. Fan and X. Peng, *Chem. Rev.*, 2016, **116**, 7768–7817.
44 H. S. Jung, P. Verwilst, A. Sharma, J. Shin, J. L. Sessler and J. S. Kim, *Chem. Soc. Rev.*, 2018, **47**, 2280–2297.
45 X. Zhao, S. Long, M. Li, J. Cao, Y. Li, L. Guo, W. Sun, J. Du, J. Fan and X. Peng, *J. Am. Chem. Soc.*, 2020, **142**, 1510–1517.
46 X. Zhao, H. Zhao, S. Wang, Z. Fan, Y. Ma, Y. Yin, W. Wang, R. Xi and M. Meng, *J. Am. Chem. Soc.*, 2021, **143**, 20828–20836.
47 Z. Zeng, S. S. Liew, X. Wei and K. Pu, *Angew. Chem., Int. Ed.*, 2021, **60**, 26454–26475.
48 Y. Zou, M. Li, T. Xiong, X. Zhao, J. Du, J. Fan and X. Peng, *Small*, 2020, **16**, e1907677.
49 S. B. Fonseca, M. P. Pereira, R. Mourtada, M. Gronda, K. L. Horton, R. Hurren, M. D. Minden, A. D. Schimmer and S. O. Kelley, *Chem. Biol.*, 2011, **18**, 445–453.
50 B. Eichhorst, M. Dreyling, T. Robak, E. Montserrat, M. Hallek and E. G. W. Group, *Ann. Oncol.*, 2011, **22**, vi50–54.
51 W. B. Mattes, J. A. Hartley and K. W. Kohn, *Nucleic Acids Res.*, 1986, **14**, 2971–2987.
52 J. A. Hartley, J. P. Bingham and R. L. Souhami, *Nucleic Acids Res.*, 1992, **20**, 3175–3178.
53 F. Song, X. Peng, E. Lu, Y. Wang, W. Zhou and J. Fan, *Tetrahedron Lett.*, 2005, **46**, 4817–4820.
54 P. Chen, J. Li, Z. Qian, D. Zheng, T. Okasaki and M. Hayami, *Dyes Pigm.*, 1998, **37**, 213–222.
55 Y. Zou, W. Liu, W. Sun, J. Du, J. Fan and X. Peng, *Adv. Funct. Mater.*, 2022, **32**, 2111853.
56 C. M. Clavel, O. Zava, F. Schmitt, B. H. Kenzaoui, A. A. Nazarov, L. Juillerat-Jeanneret and P. J. Dyson, *Angew. Chem., Int. Ed.*, 2011, **50**, 7124–7127.
57 J. Wu, R. Huang, C. Wang, W. Liu, J. Wang, X. Weng, T. Tian and X. Zhou, *Org. Biomol. Chem.*, 2013, **11**, 580–585.
58 A. Takahashi, E. Mori, G. I. Somakos, K. Ohnishi and T. Ohnishi, *Mutat. Res.*, 2008, **656**, 88–92.
59 Y. Yang, X. Fan, L. Li, Y. Yang, A. Nuernisha, D. Xue, C. He, J. Qian, Q. Hu, H. Chen, J. Liu and W. Huang, *ACS Nano*, 2020, **14**, 2509–2521.